PERGAMON

International Journal of Heat and Mass Transfer 45 (2002) 4079–4095

International Journal of HEAT and MASS TRANSFER

www.elsevier.com/locate/ijhmt

Experimental assessment of the effects of body force, surface tension force, and inertia on flow boiling CHF

Hui Zhang [a], Issam Mudawar [a,*], Mohammad M. Hasan [b]

[a] *Boiling and Two-phase Flow Laboratory, School of Mechanical Engineering, Purdue University, 1288 Mechanical Engineering Building, West Lafayette, IN 47907, USA*

[b] *NASA Glenn Research Center, 21000 Brookpark Road, Cleveland, OH 44135, USA*

Received 21 September 2001; received in revised form 26 March 2002

Abstract

The interfacial instabilities important to the modeling of critical heat flux (CHF) in reduced-gravity systems are sensitive to even minute body forces, especially for small coolant velocities. Understanding these effects is of paramount importance to both the reliability and safety of two-phase thermal management loops proposed for future space and planetary-based thermal systems. Unfortunately, reduced gravity systems cannot be accurately simulated in 1*g* ground-based experiments. However, ground-based experiments can help isolate the effects of the various forces (body force, surface tension force and inertia) which influence flow boiling CHF. In this project, the effects of the component of body force perpendicular to a heated wall were examined by conducting 1*g* flow boiling experiments at different orientations. Boiling experiments were performed using FC-72 in vertical and inclined upflow and downflow, as well as horizontal flow, and with the heated surface facing upward or downward relative to gravity. CHF was very sensitive to orientation for flow velocities below 0.2 m/s and near-saturated flow; CHF values for downflow and downward-facing heated surface were much smaller than for upflow and upward-facing surface orientations. Increasing velocity and subcooling dampened the effects of flow orientation on CHF. For saturated flow, the vapor layer characteristics fell into six different regimes: wavy vapor layer, pool-boiling, stratification, vapor stagnation, vapor counterflow, and vapor concurrent flow. The wavy vapor layer regime encompassed all subcooled and high-velocity saturated conditions at all orientations, as well as low-velocity upflow orientations. Prior CHF correlations and models were compared, and shown to predict the CHF data with varying degrees of success.

Keywords: Flow boiling; Critical heat flux; Flow orientation

1. Introduction

1.1. Reduced gravity flow boiling

New methods are being sought by government and private organizations for thermal management of heat loads in a number of space and planetary-based systems. Efficient thermal management loops are needed to transport heat from electronic, power, and environmental sources, of various sizes and power densities, to a space radiator, where the heat is ultimately rejected by radiation to deep space. This task of heat acquisition/transport/rejection can be accomplished with both single-phase and two-phase thermal management loops.

Although single-phase loops have been successfully utilized in many space applications, including NASAs Space Shuttles, focus has now shifted to the development of two-phase loops for future space systems. Two-phase loops are ideally suited for efficient removal of large heat loads since they offer better than an order of magnitude reduction in heat-load-to-weight ratio. Another merit is their ability to transport heat at nearly isothermal conditions over long piping distances. These

* Corresponding author. Tel.: +1-765-494-5705; fax: +1-765-494-0539.

E-mail address: mudawar@ecn.purdue.edu (I. Mudawar).

0017-9310/02/$ - see front matter
PII: S0017-9310(02)00133-3

Nomenclature

a	body force per unit mass perpendicular to heated surface
A_w	heated area of channel, wL
A	channel cross-sectional area
c_i	imaginary component of wave speed
c_{pf}	specific heat of liquid
D_h	channel hydraulic diameter, $4A/P_h$
g	Earth's gravitational acceleration
h_{fg}	latent heat of vaporization
k_f	thermal conductivity of liquid
L	heater length in flow direction
P_h	heated perimeter of channel (equal to w)
P_o	outlet pressure
q''	local heat flux
q''_m	CHF
T_b	calculated equilibrium bulk mixture temperature
$T_{b,o}$	calculated outlet mixture temperature
$T_{sat,o}$	saturated temperature based on measured outlet pressure
T_w	wall temperature
$\Delta T_{sub,o}$	calculated outlet sub-cooling, $T_{sat,o} - T_{b,o}$
U	liquid inlet velocity
ΔU	velocity difference between vapor and liquid
w	heater width

Greek symbols

θ	flow orientation angle
λ	wavelength of vapor layer interface
λ_c	wavelength corresponding to onset of interfacial instability
λ_d	wavelength corresponding to fastest growth of interfacial instability
ρ_f	density of saturated liquid
ρ_g	density of saturated vapor
σ	surface tension

attributes are mostly the result of the large boiling and condensation heat transfer coefficients realized with the coolant's change of phase. Earlier generation two-phase cooling systems for space exploration include heat pipes, loop heat pipes, and capillary pumped loops [1]. All three systems use capillary forces to return liquid coolant to an evaporator, where the heat is extracted from a heat-dissipating device. Since capillary forces can sustain only very small pressure drops, coolant flow rates in these systems are typically very small. This is why these three systems can only be used in relatively low heat flux and low total heat load space systems. To alleviate those performance constraints, mechanically pumped two-phase loops are becoming increasingly attractive, if not necessary.

Reduced gravity power and electronic cooling devices are mostly heat-flux-controlled. Critical heat flux (CHF) under these conditions is a highly transient phenomenon, which can lead to a sudden, large rise in the device temperature. Many materials cannot withstand this sharp temperature rise; consequently, they melt, burn out, or undergo some form of permanent damage. CHF is therefore a primary concern in the design of reduced-gravity cooling hardware. The ability to predict CHF is of paramount importance to both the reliability and safety of a space system's two-phase thermal management loop.

High cost, hardware complexity, and sparse data the researchers are able to obtain from short-duration drop-tower or parabolic flight microgravity experiments, compounded by limited access to Space Shuttle experiments, are all reasons behind the relatively small body of literature on flow boiling CHF in reduced gravity. These, and the desire to approach the understanding of boiling in reduced gravity on a very fundamental basis, explain why virtually all reduced gravity CHF studies have been focussed on pool boiling.

In a comprehensive review of pre-1967 reduced-gravity experiments, Siegel [2] found pool boiling CHF between 0.01 and 1g is proportional to $g^{1/4}$ Since most of these data were obtained in very short-duration drop-tower experiments, it was difficult to ascertain the limiting value of CHF as gravity approaches zero. Nonetheless, the large reduction in CHF in vanishing gravity is an obvious concern in two-phase thermal management loop design.

Bulk motion is an effective means for enhancing CHF relative to pool boiling. CHF in 1g flow boiling increases monotonically with increases in bulk velocity, especially under subcooled conditions [3]. Bulk motion increases CHF by flushing bubbles away from the heated surface before they coalesce to large vapor masses, and by replenishing the surface with bulk liquid. Subcooling, on the other hand, both increases the sensible energy of the replenishing liquid, and greatly reduces the size of coalescent vapor masses during intense boiling.

Unfortunately, the power "budget" in a space system is very limited since it has to be generated by batteries which are powered by solar panels. This places stringent limitations on both coolant velocity and subcooling in a two-phase thermal management loop. To minimize pumping power requirements, only very low coolant velocities can be tolerated. Additionally, the small size of loop condensers favors near-saturated coolant condi-

tions. The combination of low velocity and near-saturated flow carries the risk of producing small CHF values in reduced gravity. Unfortunately, very little is presently known about CHF under these conditions.

1.2. Critical heat flux mechanism

Recent 1g flow boiling CHF studies shed some light about the complexity of the CHF mechanism under conditions of low velocity, near-saturated flow, and reduced gravity. Galloway and Mudawar [4,5] observed vapor bubbles coalesce at 1g into a wavy vapor layer upon the heated surface as CHF is approached. Idealized in Fig. 1, the individual wavy vapor patches perfectly insulate the heated surface beneath. Heat transfer occurs mainly by vigorous boiling at wetting fronts corresponding to the troughs between the vapor patches. CHF occurs when the momentum of vapor generated by boiling in the wetting fronts exceeds the pressure force resulting from interfacial curvature. Interfacial separation ensues and the surface is covered with a continuous insulating vapor blanket.

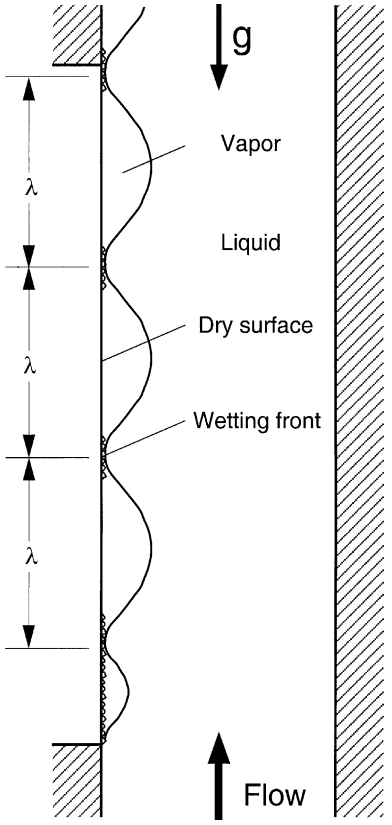

Fig. 1. Wavy vapor layer propagation along heated surface at CHF− in vertical upflow at 1g.

In their model, Galloway and Mudawar employed an interfacial instability analysis to describe the wavy motion of the vapor layer. The interface is destabilized by inertia and body force component perpendicular to the surface, while surface tension helps preserve interfacial stability. Linear instability theory yields a relation for wave speed possessing both real and imaginary components; the existence of the latter dictates if interfacial perturbations become unstable. For semi-infinite media, the interface is unstable when the interfacial wavelength, λ, exceeds a critical wavelength, λ_c, which is determined by setting the following expression for the imaginary component of wave speed equal to zero [4,5].

$$c_i^2 = \frac{\rho_f \rho_g}{(\rho_f + \rho_g)^2}\Delta U^2 + \frac{\rho_f - \rho_g}{(\rho_f + \rho_g)}\frac{1}{(2\pi/\lambda)}a - \frac{\sigma}{\rho_f + \rho_g}\left(\frac{2\pi}{\lambda}\right). \quad (1)$$

Aside from fluid properties, Eq. (1) shows the onset of instability is a function of both ΔU, velocity difference between the two phases, and a, the magnitude of body force per unit mass perpendicular to the surface. The wavelength of an unstable interface can range from λ_c to λ_d, the wavelengths corresponding to the onset of instability and fastest growth of instability, respectively; the later is determined by setting the derivative of c_i with respect to λ in Eq. (1) equal to zero. Fig. 2a and b show the variations of λ_c and λ_d, respectively, with body force, measured as number of Earth g's, for different magnitudes of velocity difference. At high g's ($a/g \gg 1$), both wavelengths follow the Taylor instability, which is dominated by a balance between surface tension and body forces. Below $a/g = 1$, wavelengths are far more complex, exhibiting different instability characteristics for different velocities. For $a/g \ll 1$, wavelengths follow the Helmholtz instability (dominated by a balance between surface tension forces and inertia) for high velocities, but for small flow velocities, wavelengths are very sensitive to even minute body forces. Furthermore, wavelengths at small velocities can become large enough to engulf an entire heat dissipating device surface, greatly increasing the likelihood of physical burnout.

In a ground-based flow boiling system, the body force term in Eq. (1) is determined by the component of the g-field normal to the heated surface, consequently, by the flow orientation. Interestingly, the above wavy vapor layer depiction at CHF− has also been confirmed for pool boiling on near-vertical surfaces [6]. A more recent study by Howard and Mudawar [7] showed the surface orientation effects can be divided into three regions: near-horizontal upward-facing, near-vertical, and downward-facing. In the near-horizontal upward-facing region, the buoyancy forces remove the vapor vertically off the heater surface in accordance with the classical

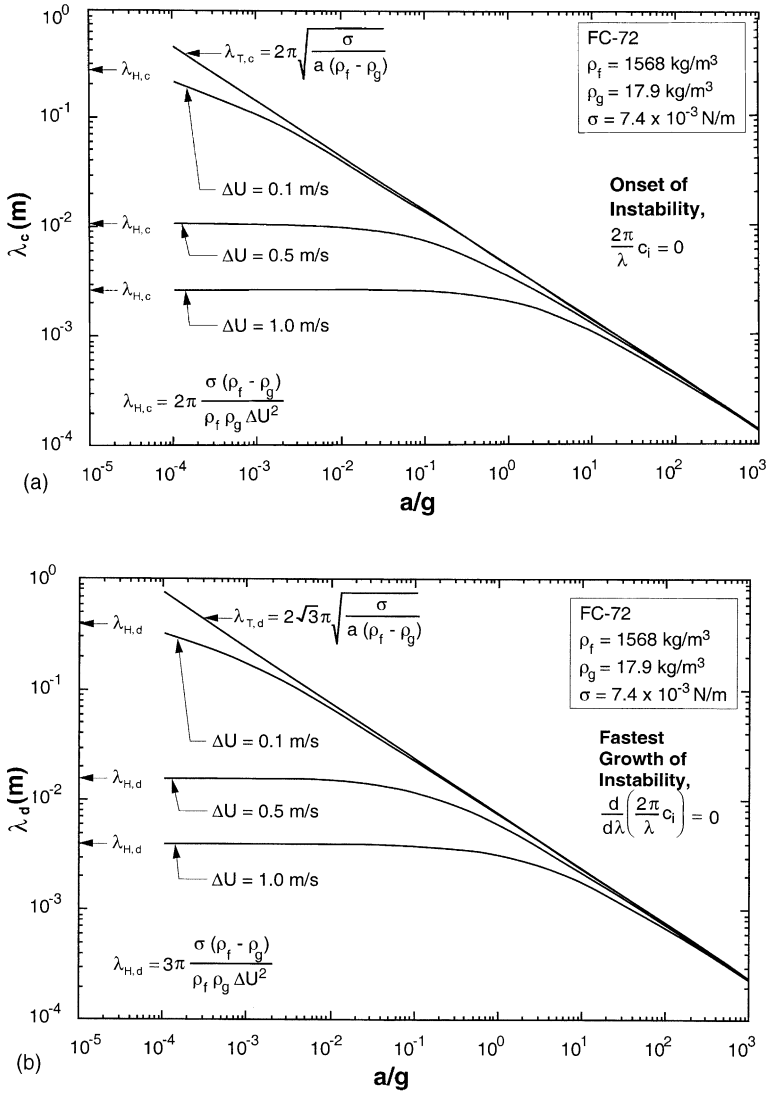

Fig. 2. Wavelength of interfacial perturbation corresponding to (a) onset of instability and (b) fastest growth of instability.

pool boiling model by Zuber et al. [8]. The near-vertical region is characterized by a wavy vapor layer sweeping along the heater surface, closely resembling the vertical flow boiling CHF illustrated in Fig. 1. In the downward-facing region, the vapor repeatedly stratifies upon the heater surface, greatly reducing CHF. These and many earlier studies [9–14] prove different models should be developed for different orientations due to the vast differences in CHF trigger mechanism for the different orientations. These results clearly demonstrate the importance of body force in modeling pool boiling CHF.

The differences in CHF trigger mechanism for different orientations become even more pronounced in flow boiling because of the complex flow interactions that may result at different flow velocities. Simoneau and Simon [15], for example, indicated vapor motion in vertical nitrogen downflow changes from concurrent at high liquid velocities to countercurrent at low velocities, and CHF values for downflow are lower than for upflow at the same velocity. Increasing the inlet velocity decreases the difference between upflow and downflow CHF due to a diminution of buoyancy effects relative to liquid inertia. Mishima and Nishihara [16] suggested flooding is the cause of CHF for downflow at very small velocities. As the velocity is increased from a flooded downflow state, the bubbles become stagnant due to a balance between the drag force exerted by the liquid and the buoyancy force. This stagnation produces an even lower CHF than flooding does at lower velocities. When the flow velocity is increased further, the bubbles be-

come entrained in the liquid and move stream-wise; CHF increases.

Gersey and Mudawar [17] studied the effects of flow orientation on flow boiling CHF in mainframe computer cooling. CHF showed significant sensitivity to flow orientation and therefore to the component of gravity (i.e. body force) normal to the heated surface. This sensitivity became weaker at higher inlet liquid velocities, and increasing subcooling served to dampen the effects of orientation even further. During the downflow tests, they observed the vapor moving counterflow (upwards) at very low velocities, becoming stagnant at slightly higher velocities, and moving with the liquid with further increases in velocity. Stratification occurred at low velocities for downward-facing horizontal surfaces.

The studies by Mishima and Nishihara [16], and Gersey and Mudawar [17] demonstrate the complexity of CHF mechanism at low velocities and different magnitudes of body force. As shown in Fig. 2a and b, low velocities produce conditions that are very sensitive to even minute body forces. The primary objectives of the present study are to: (1) explore these phenomena more rigorously, (2) capture all possible CHF regimes associated with the different orientations, and (3) assess the effectiveness of prior CHF models and correlations in predicting experimental data corresponding to the different regimes.

2. Experimental methods

2.1. Flow boiling module

A flow boiling test module was fabricated which enabled side-viewing of vapor formations along a heated surface. The module was formed by bolting together two transparent polycarbonate plastic (Lexan) plates, as shown in Fig. 3. A 5.0 mm × 2.5 mm slot was milled into the bottom plate of the test module, forming a flow channel. A side portion of the same bottom plate was milled out to facilitate the insertion of a copper heater flush with one side of the flow channel. A hydrodynamically fully developed flow was achieved by placing the heater 106 hydraulic diameters from the inlet. A honeycomb insert at the channel inlet straightened the flow and broke up any large eddies. The two test module plates were bolted together, trapping a flexible Teflon cord in a shallow slot on the underside of the top plate, providing a leak-proof assembly. Leaks around the heater surfaces were prevented by careful application of a thin film of high-temperature RTV silicone rubber. Fluid temperature and pressure were measured both upstream and downstream of the heater. The pressure was measured with 0.01% accuracy transducers.

FC-72, a 3M Company dielectric fluid recommended for cooling of electronic and power devices in space systems, was used in all the tests. Its relatively low boiling point (56 °C at atmospheric pressure) and low CHF values are both especially attractive for photographic study of the CHF mechanism because the unsteady CHF temperature excursion with this fluid is much slower than with water, which greatly reduces the danger of test module burnout.

The heater block was fabricated from a single block of 99.99% pure (oxygen-free) copper. A thin portion of the block was inserted into the lower plate of the test module as shown in Fig. 4a. The heated surface, Fig. 4b, was 2.5 mm wide and 101.6 mm along the flow direction. Heat was supplied by four 150-W cartridge heaters that were embedded in the thick protruding portion of the copper block. These cartridge heaters were powered by a single 115-W variable transformer, allowing the heat dissipation to be incremented manually during testing. The cartridge heaters were distributed symmetrically in the thick portion of the copper block to ensure even heat dissipation along the heater surface in contact with the fluid.

Local heat flux and local wall temperature were determined with five sets of Type-K thermocouples inserted strategically along the heater. Each set consisted of three thermocouples situated 1.02, 6.10, and 11.18 mm from the surface.

Assuming locally one-dimensional heat conduction through the thin portion of the copper heater inserted into the lower plate of the test module, a temperature profile was calculated using a linear squares fit to the three thermocouple readings at each of the five thermocouple locations. This profile was then used to calculate both the local heat flux, q'', and local wall temperature, T_w. Measurement inaccuracies resulted from: (1) error in the thermocouple measurement itself (following calibration), (2) thermocouple hole location, (3) small variation of the thermal conductivity of oxygen-free copper over the temperature range encountered, and (4) slight non-linearity of the temperature profile between the three thermocouples at each axial location. Propagation of error analysis gave overall uncertainties in the present heat flux and wall temperature measurements of 7.9% and 0.3 °C, respectively.

The calculation of fluid bulk temperature, $T_{b,o}$, at a particular thermocouple location along the flow direction was based on heat input up to that location and the assumption of a well-mixed flow. The inlet fluid temperature was measured by the upstream thermocouple. However, the downstream thermocouple did not provide an accurate reading of the exit temperature since void fraction at the outlet was quite large in many cases. For this reason, the mixture outlet temperature was calculated in the same manner as the bulk temperature.

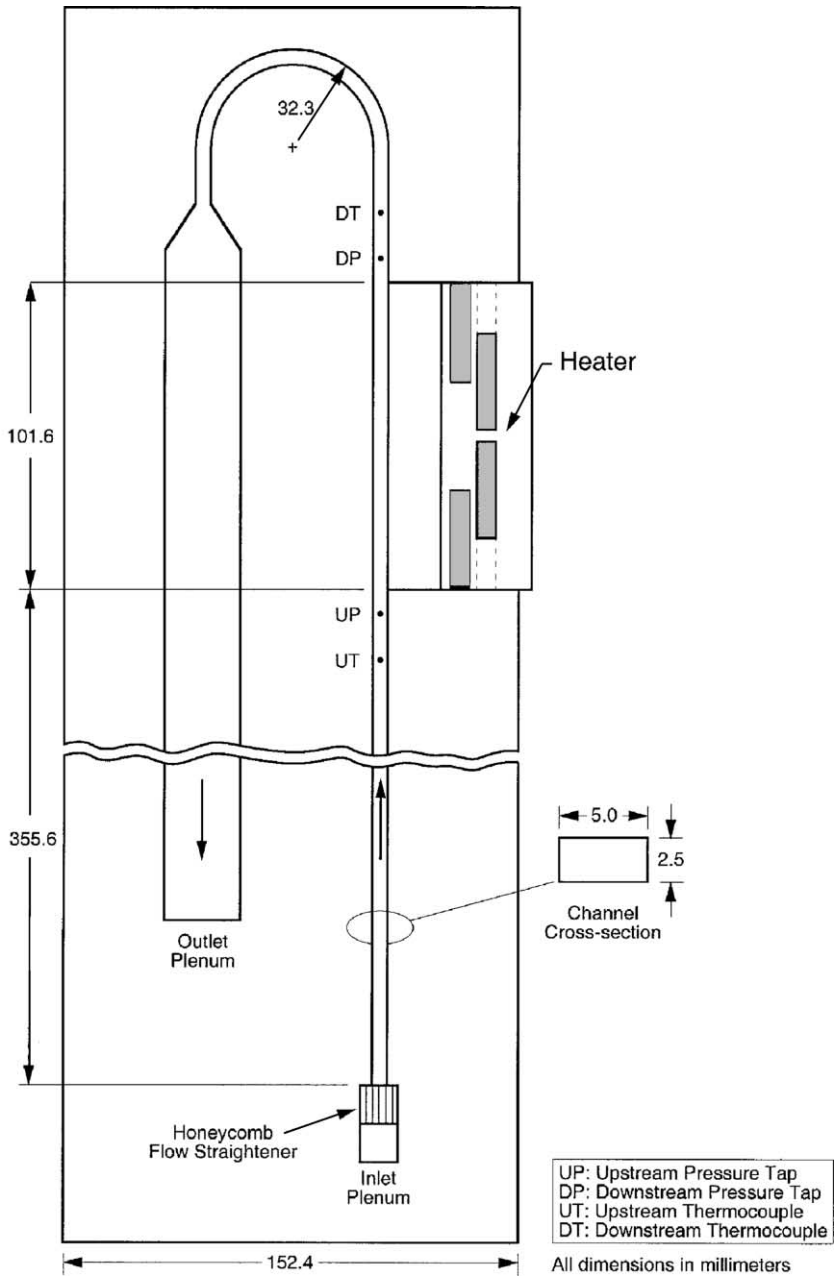

Fig. 3. Bottom plate of test module.

2.2. Flow loop

Fig. 5 shows a schematic of the two-phase flow loop that was used to supply liquid FC-72 to the test module at the desired operating conditions. Fluid flow into the channel was controlled by two valves; one of which was used to bypass excess flow. Flow rate was measured by two variable area rotameters (used mostly for visual monitoring) and a turbine flowmeter. The turbine flowmeter had a 2.3% accuracy.

The fluid temperature was modulated by a flat-plate heat exchanger and an in-line heater. The primary purpose of the heat exchanger was to cool the bulk flow from energy supplied by the test heater and the pump, using water as secondary coolant. Connected to a variable transformer, the in-line heater fine-tuned the fluid temperature prior to entering the flow channel.

The entire facility, which included the two-phase flow loop and instrumentation cabinets, was mounted onto a steel cart equipped with heavy-duty casters. This was

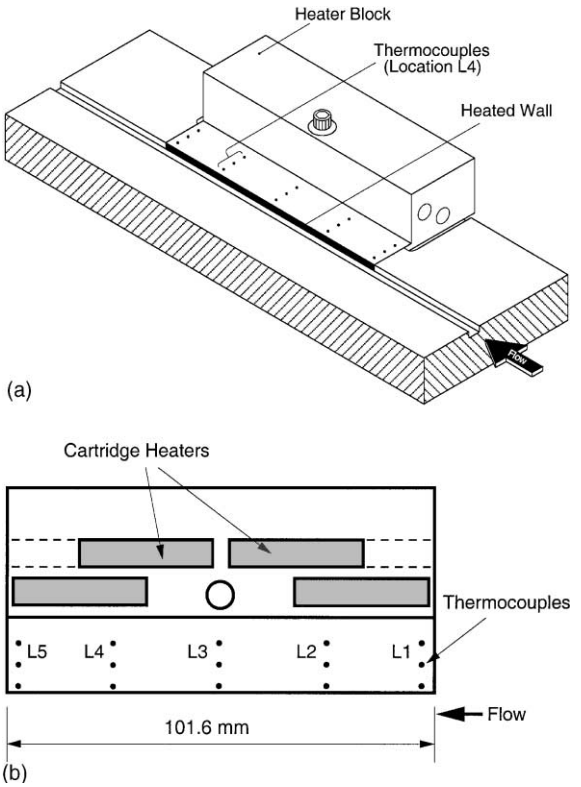

Fig. 4. (a) Heater inserted into bottom plate of test module. (b) Top view of heater.

intended to facilitate convenient transport of the facility for future parabolic flight microgravity experiments. The test module was connected to a bracket that included a 0–360° angular rotation stage, and the bracket was mounted atop the cart. The rotation stage enabled testing at all orientations relative to Earth's gravity.

2.3. Test conditions

For each test, the inlet temperature, outlet pressure, and flow rate were first adjusted to the desired test conditions with the heater electrical power set very low. Once thermal conditions became steady, a data point was recorded and electrical power incremented. Continuing in this manner, the test proceeded through the single-phase and two-phase regions generating a boiling curve, which was terminated at CHF. Steady-state conditions were evaluated based on the standard deviation of the surface temperature at thermocouple location 5. CHF is defined here as the last stable condition prior to a sudden drop in heat flux, accompanied by a sudden increase in surface temperature.

As shown in Fig. 6, tests were conducted at eight different orientations. The horizontal orientation with the heated surface facing upwards is defined as $\theta = 0°$. Moving counterclockwise, the orientation angle was increased in 45° increments to cover representative conditions for all orientations.

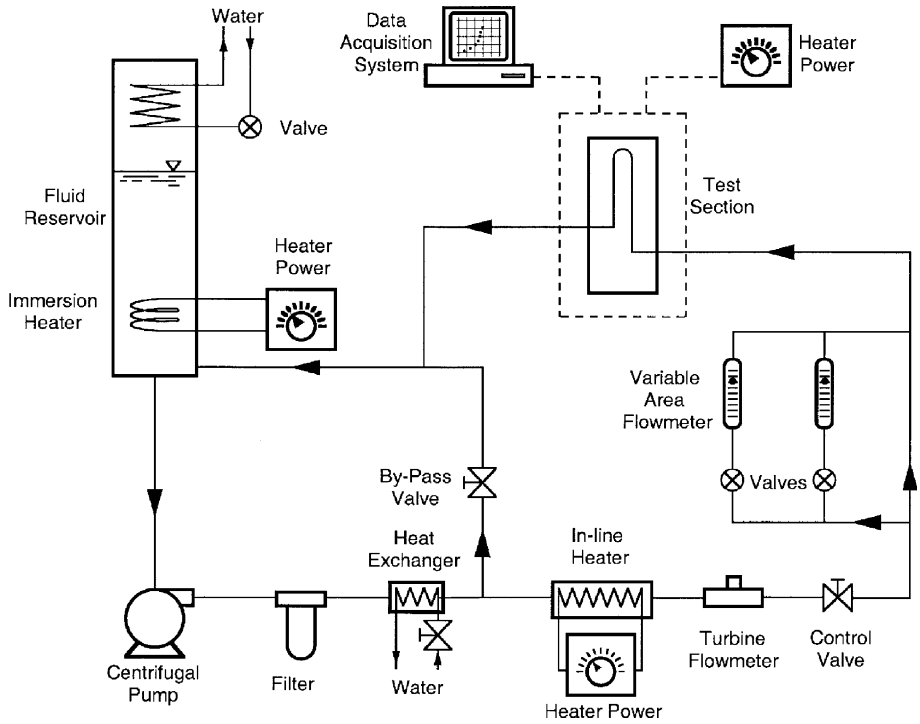

Fig. 5. Two-phase flow loop.

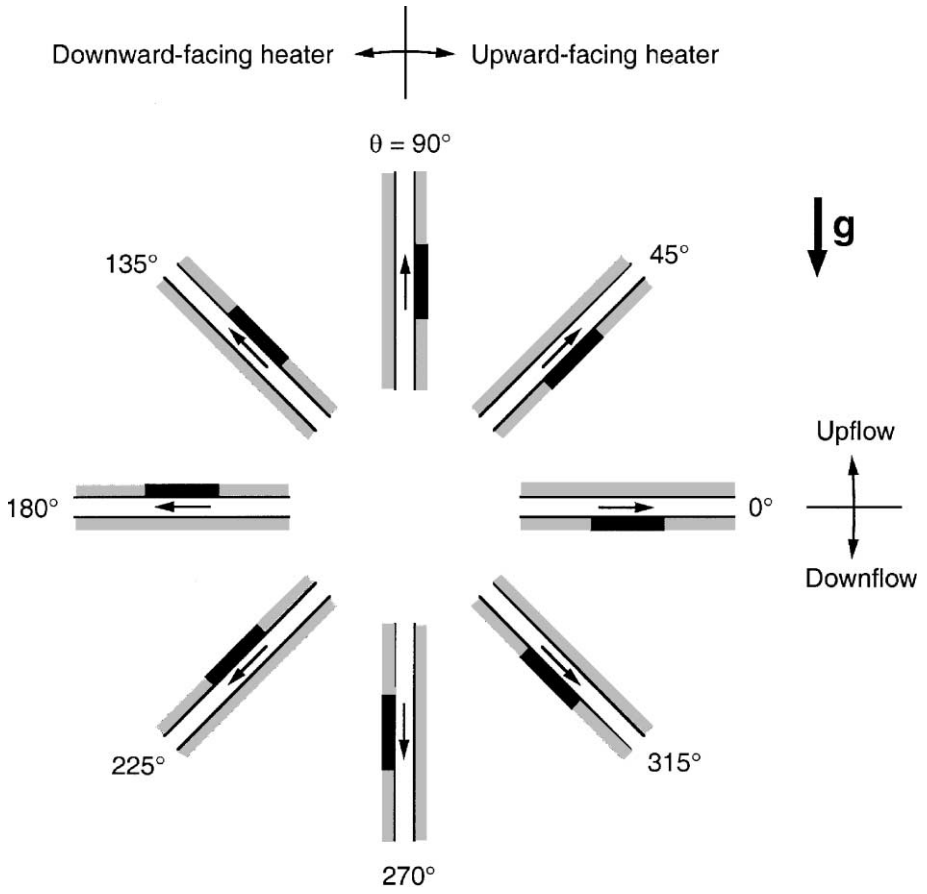

Fig. 6. Flow orientation nomenclature. Heater location for each location is indicated by solid rectangle.

For each orientation, tests were carried out at two outlet subcooling levels, referred to in this paper as saturated ($\Delta T_{sub,o} = 3$ °C) and subcooled ($\Delta T_{sub,o} = 30$ °C). For the saturated conditions, five flow velocities ($U = 0.1$, 0.2, 0.5, 1.0 and 1.5 m/s) were studied. Only three velocities ($U = 0.5$, 1.0 and 1.5 m/s) were examined. The small flow rates associated with velocities below 0.5 m/s meant the liquid had to be supplied at very low inlet temperatures to provide the desired exit subcooling. Instead of a water-cooled heat exchanger, these low inlet temperatures demand a refrigeration system, which was unavailable for the present study.

The outlet subcooling ($\Delta T_{sub,o}$) values refer to the subcooling existing at the outlet of the heated section at the time CHF was reached. The outlet pressure was held constant at $P_o = 138$ kPa (20 psia) in all tests; the corresponding saturation temperature of FC-72 is $T_{sat,o} = 66.3$ °C. Therefore, at the time CHF was reached, the outlet bulk fluid temperature was $T_{b,o} = 63.3$ °C for the saturated tests, or 36.3 °C for the subcooled.

2.4. Flow visualization techniques

The present flow visualization studies were performed with a high-speed video system using a frame rate of 1000 fps. The video camera itself was positioned to face the front side of the flow channel. The flow was back-lit by a high intensity light source. A translucent sheet of paper was placed between the light source and the channel to soften and diffuse the incoming light. Both the camera and light source were mounted on tripods, allowing both to traverse the entire heated length. All the pictures presented in this paper depict roughly the exit one-third of the heated length at CHF−, the last steady data point before the CHF transient ensued.

3. Flow visualization results

3.1. Subcooled flow

Fig. 7a shows representative CHF− photographs for a velocity of $U = 0.5$ m/s and $\Delta T_{sub,o} = 30$ °C. This is a

relatively low velocity condition, for which the liquid exerts weak drag forces upon the departing bubbles, while the high subcooling reduces bubble growth along the heated surface. At $\theta = 315°$, 0° and 45°, the buoyancy force lifted bubbles vertically upward from the heated surface into the liquid core; some stratified against the opposite wall. At $\theta = 90°$, 135°, 180° and 225°, the bubbles coalesced into wavy vapor patches which propagated along the heated surface. These wavy patches were separated by regions of liquid contact with the heated surface, resembling the CHF mechanism illustrated in Fig. 1. At $\theta = 270°$, the situation was categorically different from all other orientations. A large number of small bubbles were observed in the close vicinity of the heated surface; some coalesced and departed into the bulk liquid flow.

Vapor behavior at $U = 1.0$ m/s and $\Delta T_{sub,o} = 30$ °C was fairly similar to that shown in Fig. 7a for 0.5 m/s, the only exception being a relatively thinner vapor layer at 1.0 m/s because of the increased drag force.

Fig. 7b shows vapor behavior at CHF− for the highest flow velocity of $U = 1.5$ m/s is fairly insensitive to orientation. Wavy vapor patches with a highly ragged interface (due to increased turbulence at this high velocity) were separated by regions of more intimate liquid contact with the heated surface. Associated with this higher flow velocity is a greater drag force that helped contain the vapor in close proximity to the heated wall. The absence of any vapor bubbles in the core is also the result of the substantial subcooling, since any vapor tending to detach from the vapor patches would quickly condense into the bulk liquid. This behavior is in sharp contrast with that observed at $U = 0.5$ and 1.0 m/s for $\theta = 315°$, 0° and 45°, where coalescent bubbles slid briefly along the heater surface before detaching into the bulk flow.

3.2. Saturated flow

Fig. 8a shows vapor behavior at CHF− for the lowest flow velocity of $U = 0.1$ m/s and saturated conditions.

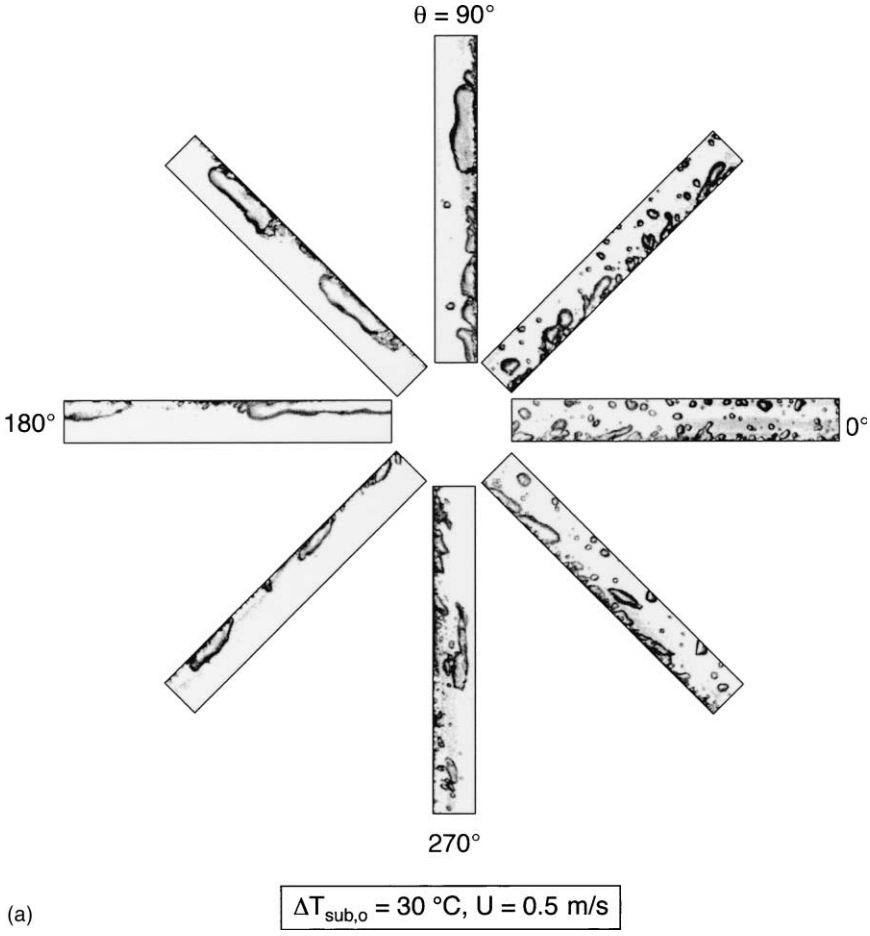

Fig. 7. Vapor behavior at $\Delta T_{sub,o} = 30$ °C for: (a) $U = 0.5$ m/s and (b) $U = 1.5$ m/s.

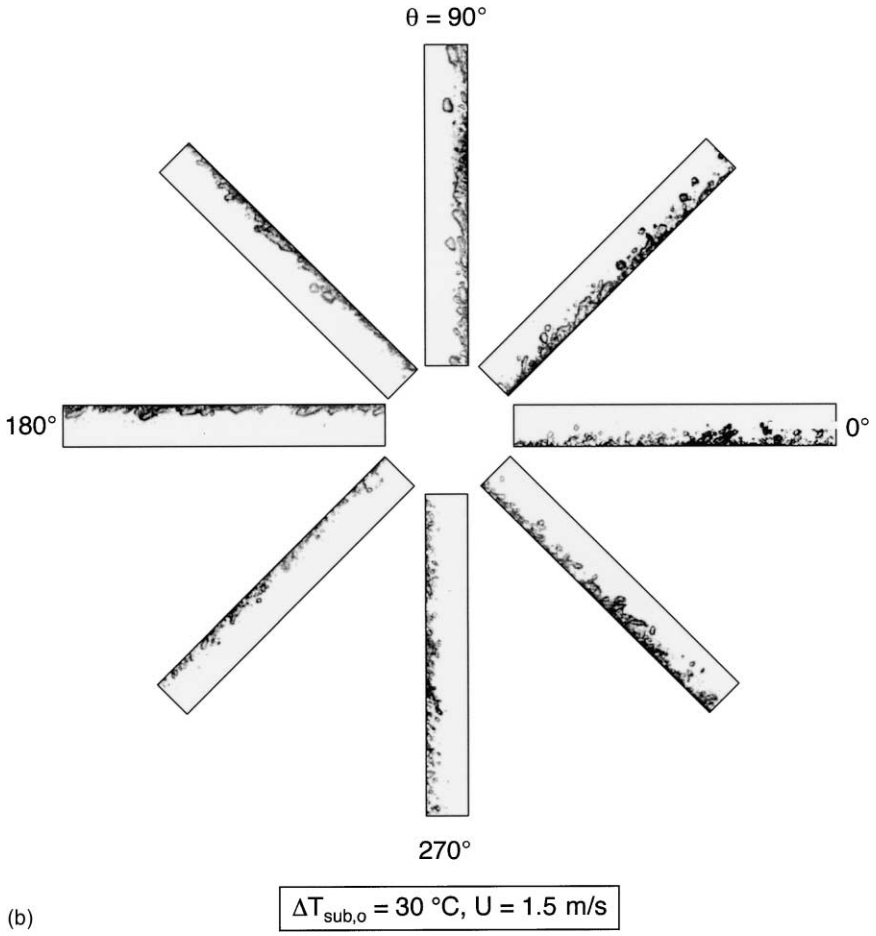

Fig. 7 (*continued*)

Clearly obvious from these photos is that CHF− is highly influenced by orientation and can be classified into several different mechanisms. For $\theta = 315°$, 0°, and 45°, boiling at this low velocity is reminiscent of pool boiling, due to the weak drag forces exerted by the liquid. Bubbles first coalesced upon the heated surface before being detached by buoyancy and driven across the channel, ultimately stratifying against the opposite wall. The $\theta = 315°$ orientation produced a very peculiar flow pattern, where bubbles coalesced into a massive vapor layer below the opposite wall as liquid ligaments flowed between the coalescent bubbles still attached to the heated wall and the massive vapor layer. For $\theta = 90°$ and 135°, a wavy vapor layer developed, allowing liquid contact between vapor patches. For $\theta = 180°$, 225°, and 270°, CHF was very small because of a drastically different vapor behavior. At heat fluxes only slightly below CHF, only a few vapor bubbles were present. Bubbles close to the heated surface moved backward relative to the incoming liquid, while those away from the surface were almost stagnant. After the heater power was increased a mere 2.4 W/cm^2, CHF commenced slowly as pronounced stratification of vapor above liquid began to take form. Bubbles developed into a thick continuous vapor blanket covering almost the entire length of the heater. This vapor blanket moved backward relative to the incoming liquid and occupied most of the channel cross-section, allowing only a thin layer of liquid to penetrate through.

Vapor behavior at a slightly higher velocity of $U = 0.2$ m/s was very similar to that at 0.1 m/s, the only difference being at $\theta = 225°$, where the massive vapor blanket was fairly stagnant relative to the incoming liquid as the drag force exerted by the liquid grew large enough to balance the buoyancy force. Stratification also occurred at $\theta = 225°$ for $U = 0.5$ m/s.

Vapor behavior at CHF− for 1.0 and 1.5 m/s was very similar, and orientation seemed to have minimal effect on the vapor layer development for both velocities. As shown in Fig. 8b for $U = 1.5$ m/s and saturated flow, the flow was dominated by wavy vapor patches sliding along the heated surface. The liquid–vapor interface was

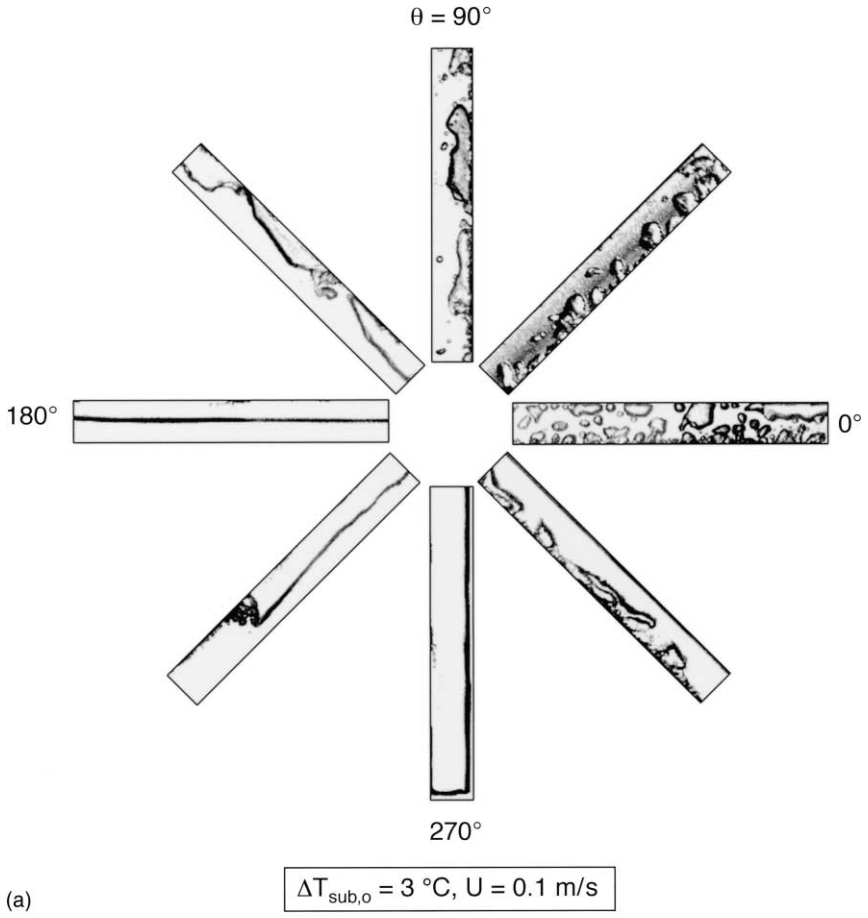

Fig. 8. Vapor behavior at $\Delta T_{sub,o} = 3$ °C for: (a) $U = 0.1$ m/s and (b) $U = 1.5$ m/s.

very ragged due to increased turbulence at this high velocity. There were also regions of liquid contact with the heated surface between the vapor patches. These observations are consistent with the CHF mechanism depicted in Fig. 1.

4. Critical heat flux results

4.1. Subcooled flow

Fig. 9a illustrates in polar form the effects of orientation on CHF for $\Delta T_{sub,o} = 30$ °C. CHF for all velocities reached maximum value at $\theta = 45°$ and decreased to a minimum at $\theta = 225°$. For $\theta = 180°$, 225°, and 270°, CHF for all velocities was lower than for the other gravity-assisted orientations; CHF decreased with the heater surface facing downward, especially in downflow. However, the effect of orientation was relatively mild for subcooled conditions, especially at the higher velocities.

4.2. Saturated flow

For the three lowest velocities of $U = 0.1$, 0.2 and 0.5 m/s and saturated flow, orientation had a very profound effect on CHF, as shown in Fig. 9b. For the upward-facing heater surface orientations, $\theta = 315°$, 0° and 45°, buoyancy helped remove vapor away from the heated surface, reducing vapor accumulation and resulting in relatively large CHF values.

For vertical upflow, $\theta = 90°$, there is no body force normal to the heated surface. Consequently, CHF values for the three lowest velocities at $\theta = 90°$ were smaller than those for the upward-facing orientations.

When the channel was turned counterclockwise further, the heated surface became downward-facing, and buoyancy forced the vapor to accumulate against the heated surface, leading to very low CHF values for $U = 0.1$ and 0.2 m/s. This is especially the case for $\theta = 180°$, with the heated surface situated completely above the fluid. For $\theta = 225°$, a combination liquid downflow and a heated surface situated above the liquid produced two undesirable effects: (1) buoyancy force

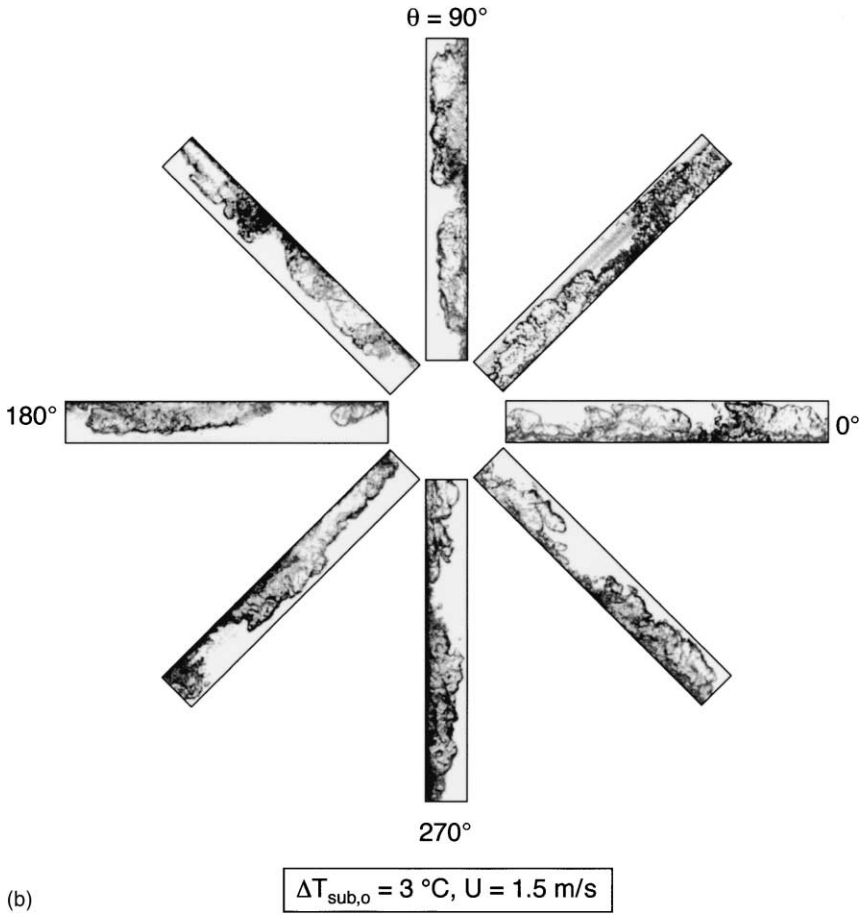

Fig. 8 (*continued*)

accumulating vapor against the heated surface and (2) buoyancy force resisting stream-wise vapor release. At times, the latter of those two effects seemed to produce a stagnant vapor mass along the heated surface because of an apparent equilibrium between buoyancy and liquid drag force. As a result of these effects, the CHF values for $U = 0.2$ and 0.5 m/s decreased further compared with those at $\theta = 180°$. But for $U = 0.1$ m/s, the buoyancy force exceeded the liquid drag force, causing the vapor to flow backwards (upwards against gravity). The ensuing vapor motion along the heated surface delayed the occurrence of CHF for $U = 0.1$ m/s at $\theta = 225°$ compared to 0.2 m/s.

For the vertical downflow orientation, $\theta = 270°$, the vapor was more capable of clearing the heated surface, in the absence of a gravity force normal to the surface, than at $\theta = 225°$. CHF values for the three lowest velocities were therefore higher at $\theta = 270°$ than at 225°.

Although the CHF values for $\theta = 135$ to 270° at the two highest velocities of $U = 1.0$ and 1.5 m/s are smaller than for other orientations, Fig. 9b shows the overall sensitivity of CHF to orientation is much weaker than at the three lowest velocities.

5. Critical heat flux regimes

The two previous sections clearly illustrate the important role of body force for different orientations and operating conditions. Body force influences both axial two-phase flow, via the body force component parallel to the heated wall, and, more importantly, interfacial instability resulting from the component of body force perpendicular to the heated wall.

The polar plots in Fig. 9a and b clearly support that notion that low velocity, near-saturated flows, which are recommended for space thermal management loops, produce the greatest sensitivity to orientation and, therefore, to the magnitude of body force perpendicular to the heated surface. The saturated data are examined here to capture all possible CHF regimes associated with the different orientations.

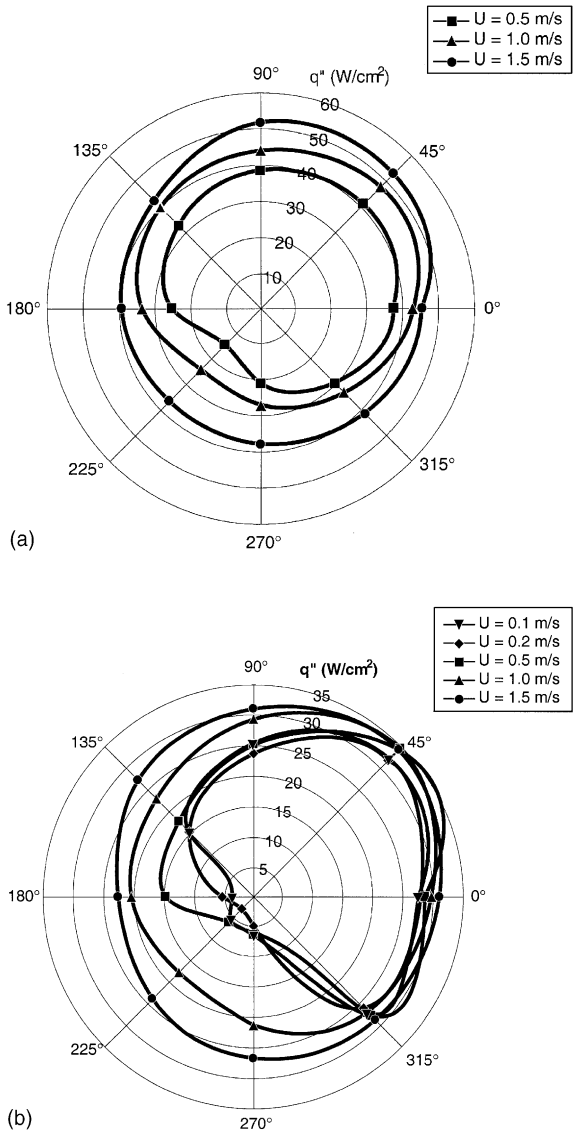

Fig. 9. CHF variation with orientation for: (a) $\Delta T_{sub,o} = 30$ °C and (b) $\Delta T_{sub,o} = 3$ °C.

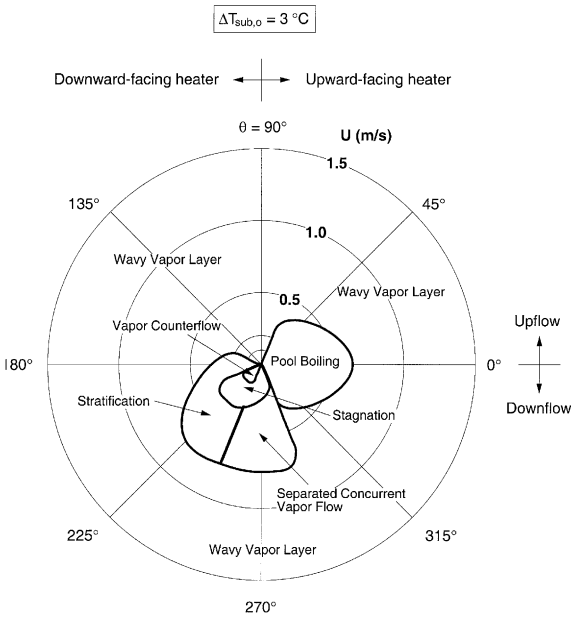

Fig. 10. CHF regimes for saturated flow.

Overall, six CHF regimes were observed with saturated flow, which are represented in polar form in Fig. 10: (1) wavy vapor layer, (2) pool boiling, (3) stratification of vapor above liquid, (4) vapor stagnation, (5) vapor counterflow, and (6) separated concurrent vapor flow.

The *wavy vapor layer* regime, which is consistent with the Galloway and Mudawar [4,5] model, is characterized by a wavy vapor–liquid interface, and liquid reaching the heated surface only in wetting fronts, located at troughs between the vapor patches. All the present $U = 1.0$ and 1.5 m/s data fall into this regime, regardless of orientation. This regime encompasses the upflow orientation at the lower velocities as well. This supports the instability hypothesis shown in Fig. 2a and b. These two figures demonstrate that, below 1*g*, interfacial instabilities at high velocities are fairly insensitive to body force, dominated by a balance between surface tension and inertia. Fig. 2a and b also prove that very low velocities greatly exasperate the effects of body force.

For the present low velocity tests with the heater surface facing upward ($\theta = 315$, 0 and 45°), a weak liquid drag force enabled buoyancy to detach coalescent bubbles into the liquid core, reminiscent of classical 1*g* horizontal pool boiling situations.

With the heater facing downward, $\theta = 180°$ and 225°, and weak liquid inertia at low velocities, buoyancy dominated the vapor formation, causing stratification of vapor above liquid. It is interesting to note that gravity becomes a stabilizing force for these orientations, evidenced by the negative body force term in Eq. (1). Instead of detaching into the liquid flow, bubbles coalesced into a thick, fairly smooth vapor layer that covered nearly the entire heated surface, and liquid penetrated through the channel as a thin stream below the vapor layer. The stratified vapor layer precluded liquid contact with the heated surface resulting in extremely low CHF values. At $\theta = 225°$, stratification was accompanied by vapor stagnation at $U = 0.2$ m/s and vapor counterflow at $U = 0.1$ m/s. The ensuing vapor motion along the heated surface increased CHF slightly for $U = 0.1$ m/s compared to 0.2 m/s.

At $\theta = 270°$, the overall shape of the vapor layer was fairly similar to that at $\theta = 180°$ and 225°, except that no

body force was exerted normal to the heated surface. In this vertical downflow ($\theta = 270°$) configuration, the vapor layer was stagnant at $U = 0.1$ m/s and moved concurrently with the liquid for 0.2 m/s. At $U = 0.5$ m/s, the vapor layer interface became highly disturbed and bubbles were observed forming in a small liquid mass at the heated surface in a predominantly separated concurrent vapor flow pattern.

Several empirical relations as well as semi-empirical and theoretical models have been proposed for CHF determination in both pool and flow boiling situations. In this study, predictions from several of those were compared to the saturated CHF data, which showed the greatest sensitivity to orientation, especially for low velocities. Five such correlations and models were examined (see Table 1): (a) pool boiling (Zuber et al. [8]), (b) flooding (Negat [18]), (c) empirical CHF correlation (Katto and Kurata [20]), (d) semi-empirical CHF model (Mudawar and Maddox [3]) developed for subcooled flow boiling of FC-72, and (e) CHF model for near-saturated flow boiling by Sturgis and Mudawar [21,22], based on the original wavy interface model by Galloway and Mudawar [4,5] illustrated in Fig. 1.

Fig. 11a compares predictions based on all the above correlations and models to the saturated CHF data belonging to the wavy vapor layer regime only, as indicated in Fig. 10. The correlation by Mudawar and Maddox [3] seems to set a lower bound for the CHF data. The Katto and Kurata [20] predictions fall below the data but approach the predictions of the Mudawar and Maddox correlation at higher velocities. The wavy vapor layer model by Sturgis and Mudawar [21,22] falls well within the data range for all velocities. CHF in this model was developed for a horizontal channel, so gravity was not accounted for. This model is based on the hypothesis of interfacial separation of vapor layer wave troughs as a result of intense boiling in these liquid contact regions. The data scatter around the model predictions is indeed the result of gravity (i.e. orientation) effects, but these effects appear relatively weak for upflow and upward-facing orientations, as well as for relatively high velocity downflow and downward-facing orientations.

Fig. 11b shows all remaining saturated CHF data corresponding to the pool boiling, stratification, vapor stagnation, vapor counterflow, and separated vapor

Table 1
CHF correlations and models

Flooding (Nejat [18], based on Wallis [19])

$$q''_{\mathrm{m}} = 0.36\left(\frac{L}{D_{\mathrm{h}}}\right)^{0.1}\left(\frac{A}{A_{\mathrm{w}}}\right)\rho_{\mathrm{g}}h_{\mathrm{fg}}\left[\frac{(\rho_{\mathrm{f}}-\rho_{\mathrm{g}})gD_{\mathrm{h}}}{\rho_{\mathrm{g}}}\right]^{1/2}\left[1+\left(\frac{\rho_{\mathrm{g}}}{\rho_{\mathrm{f}}}\right)^{1/4}\right]^{-2}$$

Developed for closed-end vertical tube; validated for water, carbon tetrachloride, ethyl alcohol, and normal hexane
Pool boiling (Zuber et al. [8])

$$q''_{\mathrm{m}} = 0.131\rho_{\mathrm{g}}h_{\mathrm{fg}}\left[\frac{\sigma g(\rho_{\mathrm{f}}-\rho_{\mathrm{g}})}{\rho_{\mathrm{g}}^2}\right]^{1/4}\left\{1+5.32\frac{\sqrt{k_{\mathrm{f}}\rho_{\mathrm{f}}c_{\mathrm{pf}}}}{\rho_{\mathrm{g}}h_{\mathrm{fg}}}\left[\frac{g\sigma(\rho_{\mathrm{f}}-\rho_{\mathrm{g}})}{\rho_{\mathrm{g}}^2}\right]^{1/8}\left[\frac{g(\rho_{\mathrm{f}}-\rho_{\mathrm{g}})}{\sigma}\right]^{1/4}\Delta T_{\mathrm{sub}}\right\}$$

Developed for infinite horizontal surfaces; validated for water, benzene, ethanol, pentane, heptane, and propane for saturated boiling, and for water and ethyl alcohol for subcooled boiling
Flow boiling CHF correlation (Katto and Kurata [20])

$$q''_{\mathrm{m}} = 0.186\rho_{\mathrm{f}}Uh_{\mathrm{fg}}\left(\frac{\rho_{\mathrm{g}}}{\rho_{\mathrm{f}}}\right)^{0.559}\left(\frac{\sigma}{\rho_{\mathrm{f}}U^2L}\right)^{0.264}$$

Valid for saturated flow boiling from a flat surface; validated for water and R-113
Semi-empirical flow boiling CHF model (Mudawar and Maddox [3])

$$q''_{\mathrm{m}} = 0.161\rho_{\mathrm{g}}Uh_{\mathrm{fg}}\left(\frac{\rho_{\mathrm{f}}}{\rho_{\mathrm{g}}}\right)^{15/23}\left(\frac{\sigma}{\rho_{\mathrm{f}}U^2L}\right)^{8/23}\left(\frac{L}{D_{\mathrm{h}}}\right)^{1/23}\left(1+\frac{c_{\mathrm{pf}}\Delta T_{\mathrm{sub}}}{h_{\mathrm{fg}}}\right)^{7/23}\left(1+0.021\frac{\rho_{\mathrm{f}}c_{\mathrm{pf}}\Delta T_{\mathrm{sub}}}{\rho_{\mathrm{g}}h_{\mathrm{fg}}}\right)^{16/23}$$

Developed for flow boiling from a flat surface in a rectangular channel; validated for FC-72
Wavy vapor layer separation CHF model (Sturgis and Mudawar [21,22] based on original model by Galloway and Mudawar [4,5])
Developed for near-saturated flow boiling from a long heated surface in a rectangular channel; validated for FC-72

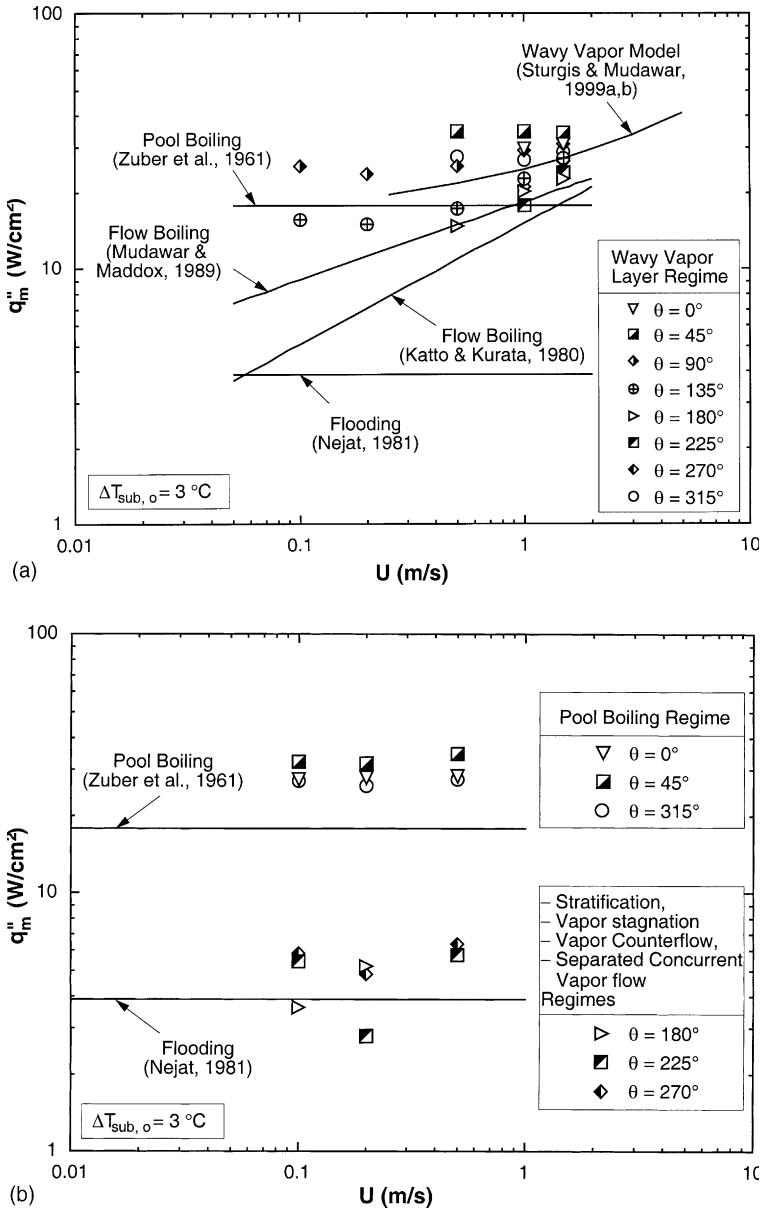

Fig. 11. Comparison of saturated CHF data with predictions of previous correlations and models. (a) Wavy vapor layer regime data. (b) Data corresponding to pool boiling, stratification, vapor stagnation, vapor counterflow, and separated concurrent vapor flow regimes.

concurrent flow regimes. Because of the added benefit of fluid motion, the pool boiling regime data are above the Zuber et al. [8] correlation developed originally for pool boiling from an infinite horizontal surface. The combination of inclined upflow and upward-facing heater surface at the 45° orientation produced the largest CHF values within the pool boiling regime. All remaining data corresponding to the stratification, vapor stagnation, vapor counterflow, and separated vapor concurrent flow regimes are considerably lower than the Zuber et al. limit, but more accurately predicted by the flooding criterion.

Fig. 12 shows all the subcooled CHF data are well distributed around the predictions of the Mudawar and Maddox [3] correlation, which was constructed for subcooled flow boiling of FC-72.

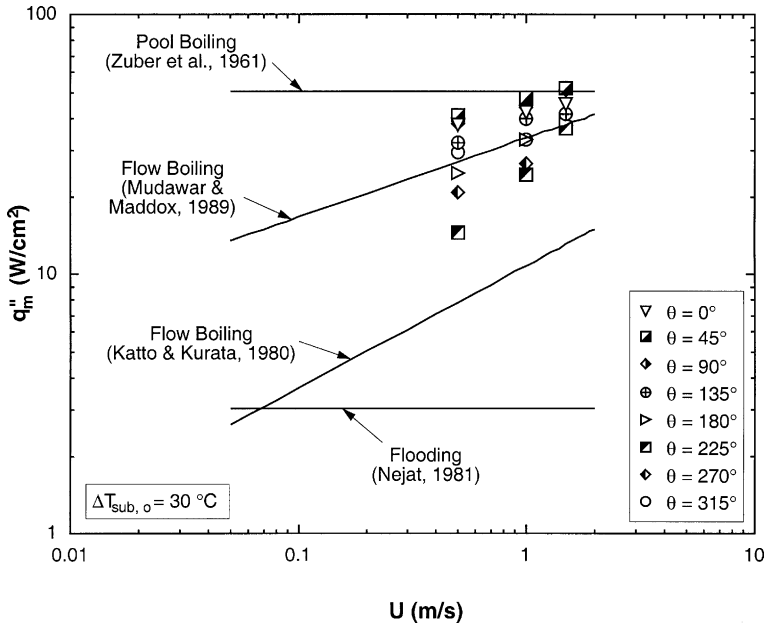

Fig. 12. Comparison of subcooled CHF data with predictions of previous correlations and models.

6. Conclusions

This study explored the effects of orientation on flow boiling CHF at saturated and subcooled conditions. Experiments were performed with coolant in vertical and inclined upflow and downflow, as well as horizontal flow, and with the heated surface facing upward or downward with respected to gravity. High-speed video imaging was also used to capture the vapor behavior at CHF− to help identify the CHF mechanism for each set of operating conditions. Key findings from this study are as follows:

(1) CHF is very sensitive to orientation for flow velocities below 0.2 m/s and saturated flow. The effects of orientation become much weaker for velocities in excess of 0.5 m/s for both saturated and subcooled flow. Increasing the subcooling serves to dampen the effects of flow orientation.

(2) At low velocities, especially for saturated flow, CHF values for downflow and downward-facing heated surface are much smaller than for upflow and upward-facing surface orientations.

(3) For near-saturated flow, the vapor layer characteristics fall into six different regimes: wavy vapor layer, pool-boiling, stratification, vapor stagnation, vapor counterflow, and vapor concurrent flow. The wavy vapor layer regime encompasses all subcooled, as well as high-velocity saturated conditions at all orientations, as well as low-velocity upflow orientations. Saturated data falling into this regime are well predicted by the Sturgis and Mudawar [21,22] model, while the subcooled data are better predicted by the Mudawar and Maddox [3] semi-empirical model. The low velocity, near-saturated upward-facing heater data are underpredicted by the Zuber et al. Model [8]. All remaining stratification, vapor stagnation, vapor counterflow, and vapor concurrent flow data seem closely related to flooding.

(4) The vast differences between the vapor layer characteristics corresponding to different CHF regimes suggest efforts to develop a single universal CHF model for all velocities, subcoolings, and orientations should be avoided. Future work should focus more on further refinement of existing models or correlations that are better suited for a particular CHF regime.

(5) The combination of low velocity and near-saturated flow in future space systems carries the risk of producing small CHF values in reduced gravity. Investigation of flow boiling CHF in reduced gravity is therefore very crucial to the safety and reliability of future space thermal management loops.

Acknowledgements

The authors are grateful for the support of the National Aeronautics and Space Administration under grant no. NAG3-2336.

References

[1] T.J. LaClair, I. Mudawar, Thermal transients in a capillary evaporator prior to the initiation of boiling, Int. J. Heat Mass Transfer 43 (2000) 3937–3952.

[2] R. Siegel, Effects of reduced gravity on heat transfer, in: J.P. Hartnett, T.F. Irvine Jr. (Eds.), Advances in Heat Transfer, vol. 4, Academic Press, New York, NY, 1967, pp. 143–228.
[3] I. Mudawar, D.E. Maddox, Critical heat flux in subcooled flow boiling of fluorocarbon liquid on a simulated electronic chip in a vertical rectangular channel, Int. J. Heat Mass Transfer 32 (1989) 379–394.
[4] J.E. Galloway, I. Mudawar, CHF mechanism in flow boiling from a short heated wall—Part 1. Examination of near-wall conditions with the aid of photomicrography and high-speed video imaging, Int. J. Heat Mass Transfer 36 (1993) 2511–2526.
[5] J.E. Galloway, I. Mudawar, CHF mechanism in flow boiling from a short heated wall—Part 2. Theoretical CHF model, Int. J. Heat Mass Transfer 36 (1993) 2527–2540.
[6] I. Mudawar, A.H. Howard, C.O. Gersey, An analytical model for near-saturated pool boiling CHF on vertical surfaces, Int. J. Heat Mass Transfer 40 (1997) 2327–2339.
[7] A.H. Howard, I. Mudawar, Orientation effects on pool boiling CHF and modeling of CHF for near-vertical surfaces, Int. J. Heat Mass Transfer 42 (1999) 1665–1688.
[8] N. Zuber, M. Tribus, J.W. Westwater, The hydrodynamic crisis in pool boiling of saturated and subcooled liquids, in: International Developments in Heat Transfer: Proceedings of International Heat Transfer Conference, Boulder, CO, 1961, pp. 230–236.
[9] C.R. Class, J.R. DeHaan, M. Piccone, R.B. Cost, Boiling heat transfer to liquid hydrogen from flat surfaces, in: K.D. Timmerhaus (Ed.), Advances in Cryogenic Engineering, vol. 5, Plenum Press, New York, NY, 1960, pp. 254–261.
[10] P.M. Githinji, R.H. Sabersky, Some effects of orientation of the heating surface in nucleate boiling, J. Heat Transfer 85 (1963) 379.
[11] W.R. Marcus, D. Dropkin, The effect of surface configuration on nucleate boiling heat transfer, Int. J. Heat Mass Transfer 6 (1963) 863–867.
[12] L.T. Chen, Heat transfer to pool-boiling freon from inclined heating plate, Lett. Heat Mass Transfer 5 (1978) 111–120.
[13] K. Nishikawa, Y. Fujita, S. Uchida, H. Ohta, Effect of heating surface orientation on nucleate boiling heat transfer, in: Y. Mori, W.J. Yang (Eds.), Proceedings of ASME-JSME Thermal Engineering Joint Conference, vol. 1, Honolulu, HI, 1983, pp. 129–136.
[14] V. Kumar, M. Prasad, M.K. Verma, N.S. Garg, Effect of inclination on pool boiling heat transfer from a flat plate, Indian Chem. Eng. 32 (1990) 61–64.
[15] R.J. Simoneau, F.F. Simon, A visual study of velocity and buoyancy effects on boiling Nitrogen, NASA Tech Note TN D-3354, 1966.
[16] K. Mishima, H. Nishihara, The effect of flow direction and magnitude on CHF for low pressure water in thin rectangular channels, Nucl. Eng. Des. 86 (1985) 165–181.
[17] C.O. Gersey, I. Mudawar, Orientation effects on critical heat flux from discrete, in-line heat sources in a flow channel, J. Heat Transfer 115 (1993) 973–985.
[18] Z. Nejat, Effect of density ratio on critical heat flux in closed end vertical tubes, Int. J. Multiphase Flow 7 (1981) 321–327.
[19] G.B. Wallis, One-dimensional two-phase flow, McGraw-Hill, New York, NY, 1969.
[20] Y. Katto, C. Kurata, Critical heat flux of saturated convective boiling on uniformly heated plates in a parallel flow, Int. J. Multiphase Flow 6 (1980) 575–582.
[21] J.C. Sturgis, I. Mudawar, Critical heat flux in a long rectangular channel subjected to one-sided heating—I. Flow visualization, Int. J. Heat Mass Transfer 42 (1999) 1835–1847.
[22] J.C. Sturgis, I. Mudawar, Critical heat flux in a long rectangular channel subjected to one-sided heating—II. Analysis of critical heat flux data, Int. J. Heat Mass Transfer 42 (1999) 1849–1862.